An Alternative Complex Boundary Element Method for Nonlinear Free Surface Problems

S.W. Hong, W.W. Schultz and W.P. Graebel
Department of Mechanical Engineering and Applied Mechanics

Contract Number N00014-86-K-0684
Technical Report No. 88-02

February 24, 1988

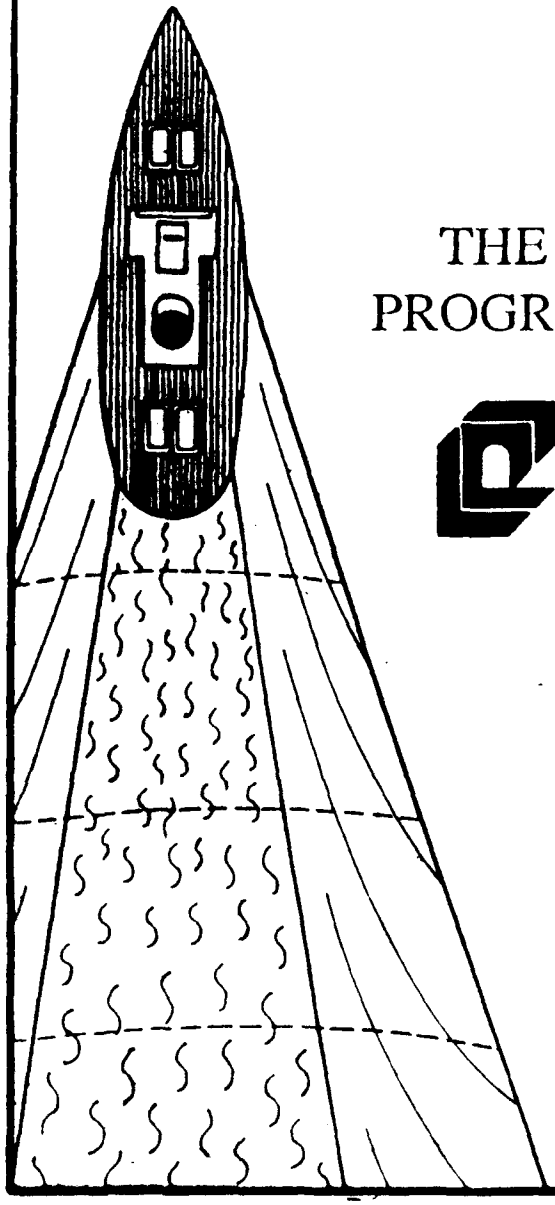

THE UNIVERSITY OF MICHIGAN
PROGRAM IN SHIP HYDRODYNAMICS

COLLEGE OF ENGINEERING

NAVAL ARCHITECTURE &
MARINE ENGINEERING

AEROSPACE ENGINEERING

MECHANICAL ENGINEERING &
APPLIED MECHANICS

SHIP HYDRODYNAMIC
LABORATORY

SPACE PHYSICS RESEARCH
LABORATORY

ERIM

Abstract

A complex variable boundary element method is developed for potential flow problems by applying Cauchy's integral theorem to the complex velocity. The resulting integral equation is a function of the normal and tangential velocity components on the boundary. A new form of the full nonlinear dynamic free surface boundary condition is used to describe the evolution of tangential velocities. This alternate method solves for flows with field singularities more easily than the conventional method, which uses the complex velocity potential. Also, the velocity field is given directly without the need for numerical differentiation. Under the new formulation, the dynamic free surface boundary condition does, however, become more complicated. As a result, while the new form of the boundary element method has definite advantages for fixed boundaries, its usefulness for free surface problems is mixed.

1 Introduction

Since Longuet-Higgins and Cokelet [1] introduced a semi-Lagrangian method for the full nonlinear initial-boundary value problem of breaking wave simulation, a number of different numerical models for fully nonlinear free surface problems have been developed, e.g., Vinje and Brevig [2]; Baker, Meiron and Orszag [3]; Dold and Peregrine [4]; etc. Longuet-Higgins and Cokelet [1] used Green's theorem to develop an integral equation for the normal velocity, $\frac{\partial \phi}{\partial n}$, when the velocity potential, ϕ, is given as an initial condition on the free surface. Vinje and Brevig [2] applied Cauchy's integral theorem to the complex potential ($\beta = \phi + i\psi$) to form an integral equation for ψ. Baker, Meiron, and Orszag [3] developed a method wherein the velocity field is represented by distributed vortices (or dipoles) along the free surface. The time evolution of the vortex sheet strength is found by solving an integral equation. In all these cases, numerical differentiation or integration is needed to obtain the velocity on the free surface.

Martensen [5] and Lewis and Ryan [6] employed boundary element methods directly to determine the velocity on boundaries. Their work was not extended to free surface problems. Recently, Dold and Peregrine [4] used a boundary element method to directly compute the complex velocity (κ) based on Cauchy's integral theorem. Their form of the dynamic free surface boundary condition is based on the velocity potential, so recalculation of the rate of change of the velocity potential following a material particle was necessary.

In real flows, viscosity generates vorticity at the surface of solid bodies. This vorticity is shed, resulting in an unsteady wake flow. Vortex methods (e.g., [7]) assume that vorticity is shed as discrete vortices or as a vortex sheet in an otherwise irrotational flow. In the two-dimensional problem, the velocity potential of the shed vortices is multivalued (i.e., the domain has branch cuts). Special care and treatment is therefore needed to incorporate these vortices into velocity potential boundary element methods.

An alternative two-dimensional boundary element model for complex velocity is derived here, together with a modified dynamic boundary condition on the free surface in terms of the velocity. The advantages and disadvantages are discussed, and some simple computational examples are given.

2 Formulation using Cauchy's Theorem

Usually Cauchy's theorem is applied to the complex potential to derive a complex variable boundary element method for irrotational flow problems. Here, we use Cauchy's theorem to derive an integral equation in terms of the complex velocity. Let the complex velocity of the problem be κ, which is analytic inside the domain and is given as

$$\kappa = u - iv \,, \tag{1}$$

where u and v are the velocity components in the x and y directions, respectively.

Figure 1 shows the problem domain and bounding surfaces. Cauchy's theorem gives

$$\oint_{\partial\Omega} \frac{\kappa(z)}{z - \zeta_k} dz \;=\; i\alpha\kappa(\zeta_k) \,, \tag{2}$$

where α is 0 or 2π when the location of the kernel singularity, ζ_k, is outside or inside the boundary, respectively. If the kernel singularity is on the boundary ($\zeta_k \in \partial\Omega$), α is equal to the included angle, and the integral is treated as principal-valued. We take ζ_k to approach the boundary from the outside of the domain so that α is zero. The algebraic system is formed from (2) by discretizing the integral and letting the kernel singularity approach each of the N nodal points in turn, i.e. $\zeta_k \rightarrow z_k$. A special limiting process is needed to evaluate the integral near ζ_k.

The boundary contour, $\partial\Omega$, is decomposed into $\partial\Omega_n$ and $\partial\Omega_s$, where the normal velocity is given on $\partial\Omega_n$ and the tangential velocity is given on $\partial\Omega_s$. For a free surface time marching problem, $\partial\Omega_n$ would represent a solid surface and $\partial\Omega_s$ a free surface. Hence, the boundary conditions can be categorized by the following given conditions:

$$Re\{\kappa e^{i\theta}\} = V_s \qquad on\ \partial\Omega_s\ , \tag{3}$$

$$Im\{\kappa e^{i\theta}\} = V_n \qquad on\ \partial\Omega_n\ . \tag{4}$$

Here θ is the tangent angle with respect to the positive x axis as shown in Figure 1.

The boundary contour is represented as piecewise-linear panels and the complex velocity as piecewise-linear functions in a panel. z_j and κ_j denote the location and complex velocity at the jth node point. Our numerical model assumes that κ on the jth panel is of the form

$$\kappa(z) \;=\; \frac{1}{z_{j+1}-z_j}\,[\kappa_j(z_{j+1}-z)+\kappa_{j+1}(z-z_j)\,]\ . \tag{5}$$

Exact integration of (2) with approximation (5) gives

$$\sum_{j=1}^{N}\kappa_j\Gamma_{jk} \;=\; 0 \qquad for\ k=1,\ldots,N\ , \tag{6}$$

where

$$\Gamma_{jk} \;=\; \frac{z_{j+1}-\zeta_k}{z_{j+1}-z_j}\,\ln(\frac{z_{j+1}-\zeta_k}{z_j-\zeta_k}) \;-\; \frac{z_{j-1}-\zeta_k}{z_j-z_{j-1}}\,\ln(\frac{z_j-\zeta_k}{z_{j-1}-\zeta_k})\ ,\ for\ j\neq k \tag{7}$$

and

$$\Gamma_{kk} \;=\; \ln(\frac{z_{k+1}-\zeta_k}{z_{k-1}-\zeta_k})\ . \tag{8}$$

Equation (7) is evalutated using L'Hospital's rule when j is either $k+1$ or $k-1$.

The total complex velocity can be written as

$$\kappa = \kappa_I + \kappa_v + \kappa_d\ , \tag{9}$$

where subscripts I, v, and d denote the components due to the incoming flow, the free vortices, and the remainder (i.e., body and free surface singularities), respectively. Usually in a problem κ_I and κ_v will be given, and κ_d will be unknown.

The complex velocity due to vortices is given by

$$\kappa_v = \frac{1}{2\pi i} \sum_{j=1}^{N_v} \frac{\gamma_j}{(z - z_{v_j})} , \tag{10}$$

where γ_j is the strength of a vortex located at z_j, and N_v is the total number of vortices. Note that the complex velocity of a vortex is single-valued, but its complex potential is not. The complex velocity potential of a vortex or source is given as a logarithmic function, the imaginary part of which is multi-valued. Hence, in the conventional potential method we have difficulty in uniquely satisfying the boundary conditions due to branch cuts. This is also true for the integral equation formulation using Green's theorem.

We apply Cauchy's theorem to κ_d instead of κ, since κ_d is expected to go to zero far from the region of disturbance. We could instead apply the residue theorem to $\kappa_d + \kappa_v$, but the present method is computationally equivalent. In either case, the contour integration contribution in the far field will be eliminated. The disturbance from a solid body dies out as $O(1/z^2)$, but the disturbance at a free surface does not decay, due to travelling waves. To make the computational domain finite, either spatial periodicity is assumed or an initial-value problem is studied for small time such that the free surface disturbances are confined to a small region. Alternatively, damping-layers (Baker et al. [8]) can be used to artificially dampen the far field effects on the free surface.

The total complex velocity on the contour can be rewritten in terms of the total normal and tangential velocity as

$$\kappa \, e^{i\theta} \; = \; V_s \; + \; i \, V_n \; . \tag{11}$$

Rewriting equation (6) in terms of κ_d gives the following algebraic equation in terms of V_{ds} and V_{dn}:

$$\sum_{j=1}^{N} (V_{ds} + i \, V_{dn})_j R_{jk} \; = \; 0 \qquad for \; k = 1, \ldots, N \; , \tag{12}$$

where $R_{jk} \; = \; \Gamma_{jk} e^{-i\theta_j}$, and V_{ds} and V_{dn} are the tangential and normal disturbance velocity components, respectively. Either V_{ds} or V_{dn} is specified on the boundary contour by the boundary

conditions.

The above set of complex algebraic equations gives twice as many real equations as unknowns. It is sufficient to solve half of the set of equations, say, just the real part of (12). Instead, we elect to solve all of the equations in a least-squares sense with the increased accuracy shown in Schultz and Hong [9].

3 Free Surface Boundary Conditions

The kinematic and dynamic boundary conditions of a free surface for an inviscid flow are given as

$$\frac{Dz}{Dt} = \kappa^* \,, \tag{13}$$

$$\frac{D\phi}{Dt} = -gy + \frac{1}{2} \mid \nabla\phi \mid^2 \tag{14}$$

where * denotes the complex conjugate, $\frac{D}{Dt}$ represents a material derivative, and g is the acceleration due to gravity (acting here in the $-y$ direction). The kinematic condition assures that material particles remain on a free surface. The dynamic boundary condition is the unsteady Bernoulli equation, requiring that pressure be constant along a free surface.

Since our boundary integral formulation is written in terms of the velocity, the dynamic boundary condition should be as well. The Euler equation can be written as

$$\frac{D\vec{V}}{Dt} = -\frac{\nabla p}{\rho} - g\vec{j} \,.$$

Since the pressure gradient along the free surface is zero, multiplication by the unit tangent vector $\vec{e_s}$ gives

$$\frac{DV_s}{Dt} = -V_n \frac{D\vec{e_n}}{Dt} \cdot \vec{e_s} - g\frac{\partial y}{\partial s} \,.$$

The first term on the right-hand side results from the local coordinate system being noninertial.

Rewriting this equation in terms of θ gives

$$\frac{DV_s}{Dt} = -V_n \frac{D\theta}{Dt} - g \sin\theta \ . \tag{15}$$

Thus, the rate of change in the tangential velocity following a material particle on the free surface is given by (15) as a function of the normal velocity, the tangent angle θ, and the rate of change of θ following a material particle ($\frac{D\theta}{Dt}$). Since there is a time derivative term on the right-hand side, equation (15) is not in a standard form for applying a time marching scheme.

The material derivative of the tangent angle, $\frac{D\theta}{Dt}$, can be calculated from the normal and tangential velocity distribution along a free surface by (Hong, Tryggvason, and Schultz [10])

$$\frac{D\theta}{Dt} = -\frac{\partial V_n}{\partial s} + \frac{V_s}{R} \ . \tag{16}$$

Here, R is the radius of curvature of the boundary contour and is defined as positive when the center of curvature is located on the left-hand side as we follow the contour s.

Equation (16) has the disadvantage of requiring two spatial derivatives of the contour to find the radius of curvature. For the highly deformed free surface contour, the numerical error in calculating the curvature can be very large, unless a high-order approximation is used. Our free surface computations using (15) and (16) were satisfactory only when the free surface curvatures were small. Here, we avoid the difficulty of performing two spatial derivatives to find R, by using another approximation scheme described below.

Since the present method uses the tangential and normal velocity components, the definitions of the tangent angle, θ, and the time rate of change of the tangent angle, $\frac{D\theta}{Dt}$, are crucial to the overall accuracy. We approximate the tangent angle at the jth node θ_j as

$$e^{i\theta_j} = \frac{e^{i\bar{\theta}_{j-1}} D_j + e^{i\bar{\theta}_j} D_{j-1}}{|e^{i\bar{\theta}_{j-1}} D_j + e^{i\bar{\theta}_j} D_{j-1}|} \tag{17}$$

where

$$e^{i\bar{\theta}_j} = \frac{z_{j+1} - z_j}{D_j} \ , \tag{18}$$

and D_j is the length of the jth panel. Hence, the tangent angle at a node is given by a weighted average of the mean tangent angle of the adjacent panels.

A similar procedure is taken to approximate the time rate of change of the tangent angle. $\frac{D\theta}{Dt}$ at node j is approximated by the weighted average of $\dot{\bar{\theta}}_{j-1}$ and $\dot{\bar{\theta}}_j$ as

$$\frac{D\theta_j}{Dt} = \frac{\dot{\bar{\theta}}_{j-1} D_j + \dot{\bar{\theta}}_j D_{j-1}}{D_j + D_{j-1}} , \tag{19}$$

where

$$\dot{\bar{\theta}}_j = Im\left\{\frac{\dot{z}_{j+1} - \dot{z}_j}{z_{j+1} - z_j}\right\}$$

is the time derivative of $\bar{\theta}_j$ given by (18). We find (19) to be much more accurate than (16) when piecewise linear-panels are used.

4 Numerical Calculation and Examples

The algorithm is tested on three examples to demonstrate its usefulness and accuracy. Following Longuet-Higgins and Cokelet [1], an initial-boundary value problem is defined for each case such that V_s is given on a free surface as an initial condition and V_n is given on the solid body surface.

We use a fourth-order Runge-Kutta-Gill scheme to evolve the free surface variables. The overdetermined matrix problem is solved using an iterative conjugate gradient method [11]. This solver is very efficient when a good initial guess is available, as in time marching problems.

The first example is a numerical simulation of a propagating, nonlinear gravity wave. The results of the present method are compared with the potential method. The second example is a vortex pair and wall interaction problem. The last example studies a vortex pair interacting with a free surface. For the second and last example, no comparisons are made with the potential method due to the expected difficulties of using the potential method for the field vortices problem, as mentioned in section 2.

4.1 Nonlinear Wave Simulation

A deep water, periodic, nonlinear gravity wave problem is solved using the present method and the results are compared with those of the complex potential boundary element method (Schultz [12]).

The initial surface elevation, complex potential, and corresponding tangential velocity are given in Table 1. Initial nodes are spaced uniformly in the x direction. Since this problem is periodic in x, the computational domain is reduced to a finite region in the x direction using conformal mapping [12]

$$\zeta = exp(-2\pi i\ z/\lambda), \tag{20}$$

where λ is the wavelength.

Error distributions in the x and y velocity components at the initial time are compared for the two methods in Figures 2a and 2b. A central difference scheme is used to calculate the velocity in the potential formulation. The velocity formulation is seen to give slightly better results, but the accuracy of both methods is consistent with the precision of the calculation.

In Figures 3a, b, c, and d, the time variation of the maximum surface elevation (Y_{max}), the minimum surface elevation (Y_{min}), the mass conservation (E_m), and the total energy ($E(t)$) is shown for both methods. Here E_m and $E(t)$ are defined by

$$E_m = \int_0^\lambda \eta(x,t)\ dx \Big/ \left\{ \int_0^\lambda \eta^2(x,0)\ dx \right\}^{\frac{1}{2}} \tag{21}$$

$$E(t) = \frac{1}{2} \int_0^\lambda \eta^2(x,t)\ dx + \oint \phi\ d\psi, \tag{22}$$

where $\eta(x,t)$ is the surface elevation. For the energy computations, the complex velocity potential is estimated by integrating the complex velocity along the free surface. We use 80 elements and

a time step of 0.2. The time step is sufficiently small such that time discretization errors are negligible compared to spatial discretization errors.

The potential method is more accurate for short times than the velocity method for total energy conservation, while both methods show good agreement for the other physical and error quantities. After two wave periods, however, the initial energy level is recovered in the velocity formulation. In the velocity formulation, the complex velocity must be integrated numerically in order to determine the kinetic energy. We can integrate κ analytically in a panel, because linear variation of κ in the mapped domain is assumed in the panel. Other integrating schemes using B-spline interpolation resulted in a maximum energy loss which is twice as large. Hence, we expect that high-order discretization of the Cauchy's integral will improve energy conservation.

The present method is very sensitive to the computation of the tangent angle. As the non-linear free surface wave evolves, the local curvature can be very large, so the reliability of the present scheme can deteriorate. This difficulty may be resolved by adopting a carefully chosen remeshing scheme.

Figure 4 shows the results of a convergence test for E_m and the energy conservation criteria, E_e, at fixed time t=1.0. This test increases the number of elements N from 20 to 80 while holding the time step fixed at $\Delta t = 0.1$. E_e is defined as

$$E_e = \{E(t) - E(0)\}/E(0) . \tag{23}$$

Both methods show very good (and identical) convergence for the mass conservation criteria, but poorer convergence for energy conservation. These examples also show that the velocity formulation requires slightly more computational time (2 percent) than the potential method, due to the need to calculate the tangent angle and the material derivative of the tangent angle.

4.2 Vortex Pair and Wall Interaction

As another example, the convection of a vortex pair approaching a solid wall is examined to test the accuracy of the numerical algorithm. The exact solutions for the induced velocity and the path of the vortex pair are given in Milne-Thomson [13]. Since the tangent angles on the boundary contour (solid wall) are fixed in this example, the errors in the approximation of the tangent angle (as in section 4.1) are eliminated.

The computational domain is reduced to a finite one by solving a periodic problem with a period sufficiently long so that the periodic boundary effects are negligible. The conformal mapping of the first example is again used. The initial location and strength of the vortex pair are given in Table 2 along with the imposed period.

Figure 5 shows the initial error in tangential velocity using 40 equally spaced elements. The error is normalized by the solution maximum. It shows that the present scheme gives an average error norm of one part in 10^{-6}.

The convergence rate of the tangential velocity is examined by plotting the root mean square error (E_2) as a function of the number of elements (N) using log-log scales shown in Figure 6. Surprisingly, the present scheme is fourth-order accurate in this example. Usually, the results of the linear approximation are second-order accurate. This higher convergence rate can be attributed to the use of an overdetermined system on a circular (after conformal mapping) domain [9].

On the other hand, the tangential velocity by the potential formulation is only second-order accurate. This problem can also be solved by the potential formulation, because the influence of the vortices on the wall boundary condition (ψ) is uniquely given. Even if the velocity potential calculated by the potential formulation were fourth-order accurate, the accuracy would be low-

ered by numerical differentiation (second-order central difference) to get the disturbance velocity components. The total velocity field in this case is calculated as the sum of the numerically calculated disturbance velocity and of the direct contribution from the field vortices.

The computed path of the vortex pair in time is given in Figure 7 along with the analytic solution. This shows that the time stepping method used in the present study is sufficiently accurate to follow the convected motion of the vortex pair.

4.3 Vortex Pair and Free Surface Interaction

Our final case examines a vortex pair interacting with a free surface. Initially the vortex pair is introduced into the fluid with the free surface undisturbed. Except for the vortex pair, the fluid is assumed to be irrotational.

In a potential formulation, the free surface boundary condition is given by the velocity potential. But the velocity potential due to vortices is multivalued, as we discussed in section 2. To treat this multivalued potential in the numerical computation, a carefully determined logical statement must be used. For an arbitrary boundary contour, it is difficult to devise an efficient logical statement for uniqueness. Moreover, when the vectorization of the computer code is desirable, we cannot use a logical statement. Hence, only the result of a velocity formulation is shown here.

In order to reduce the computational domain to a finite one, damping layers are introduced on both ends of computational domain following Telste's example [14]. The initial conditions and strength of the vortex pair are given in Table 3. Initially, nodes are distributed using a cosine spacing so that more material points are located near the origin. This ensures adequate spatial resolution near the origin for a short time, since the continuous upwelling of the free surface

convects nodes away from the counter-rotating vortices.

In Figure 8, the free surface elevations at $t = 13.4164$ are given. The results of Telste [14], using Baker's [3] generalized vortex method with damping layers, are in good agreement with our's, although we use a much smaller number of nodes ($N = 81$ compared to 641). Unlike the example in section 4.1, the Lagrangian movement of the nodes grows rapidly as the vortex pair approachs the free surface. Hence, a remeshing scheme of free surface nodes is needed for a reliable solutions at longer times.

5 Conclusions

A velocity form of the complex variable boundary element method was developed for potential flow by applying Cauchy's integral theorem to the complex velocity. A new form of the full nonlinear dynamic free surface boundary condition was derived as a function of the normal and tangential velocity components and successfully applied to three examples.

The main advantage of the present method over the conventional potential method is that it can more easily solve for flow with field (free) singularities such as vortices and sources. The present method also gives the velocity field directly without the need for numerical differentiation. However, it is very sensitive to the definition of the local tangent angle of the free surface so that remeshing and filtering are necessary to assure a reliable, stable solution. Specifically, the velocity formulation does not conserve energy as accurately as the potential formulation for free-surface problems without vorticity. This could be due to errors in determining the local tangent angle or in determining the velocity potential by numerical integration, which is required for the kinetic energy calculation.

Acknowledgements

This work was partially supported by Naval Research Laboratory Contract No. N00014-85-K-Z019, ONR Contract N00014-87-0509, and the Program in Ship Hydrodynamics at The University of Michigan, funded by the University Research Initiative of the Office of Naval Research, Contract No. N000184-86-K-0684. The authors acknowledge G. Trygvasson for his suggestions.

References

1. M.S. Longuet-Higgins and C.D. Cokelet, "The deformation of steep surface waves on water: I. A Numerical Method of Computation," *Proc. R. Soc. London, A350*, 1-26 (1976).

2. T. Vinje and P. Brevig, "Numerical calculations of forces from breaking waves," *Hydrodynamics in Ocean Engineering*, Norwegian Inst. Tech., 547-565 (1981).

3. G.R. Baker, D.I. Meiron and S.A. Orszag, "Generalized vortex methods for free-surface flow problems," *J. Fluid Mech. 123*, 477-501 (1982).

4. J.W. Dold and D.H. Peregrine, "Steep unsteady water waves: An efficient computational scheme," 19th Int. Conf. on Coastal Engineering, Houston (1984).

5. E.Martensen, *ARMA, 3*, 235-270 (1959) (in German).

6. R.I. Lewis and P.G. Ryan, *J. Mech. Eng. Sci., 14*, 280 (1972).

7. A. Leonard, "Vortex methods for flow simulation," *J. Comp. Phys. 37*, 289-335 (1980).

8. G.R. Baker, D.I. Meiron, and S.A. Orszag, " Generalized Vortex Methods for Free-Surface Flow Problems; II Radiating Waves," submitted for publication (1986).

9. W.W. Schultz and S.W. Hong, "Solution of potential problems using an overdetermined complex boundary integral method," submitted for publication. (1988)

10. S.W. Hong, G. Tryggvason and W.W. Schultz, "A note on the formulation of free surface problems. An integral equation for velocity," submitted for publication. (1987)

11. R. Fletcher and C.M. Reeves, *Computer Journal, 7*, 149-154 (1964).

12. W.W. Schultz, *Proceedings of 11th IMACS World Congress 2*, Oslo, Norway (1985).

13. L.M. Milne and C.B.E. Thomson , *Theoretical Hydrodynamics*, The University Press, Glasgow. (1968)

14. J.G. Telste, "Potential flow about the counter rotating vortices approaching a free surface," submitted for publication. (1987)

Table 1: Initial Conditions and Other Parameters for Nonlinear Free Surface Problem

Imposed Period	2π
Domain of Problem	$0 \leq x \leq 2\pi$
Length Scale L	Period/2π
Velocity Scale	$(gL)^{\frac{1}{2}}$
Surface Elevation	$y(x) = a \sin x$
Complex Potential	$\beta = a\ e^{-i\ (x+iy)}$
Tangential Velocity	$a\ e^{y}(\sin x - a\cos^2 x)/(1 + a^2\cos^2 x)^{\frac{1}{2}}$
Amplitude	a=0.2

Table 2: Initial Conditions and Other Parameters for Wall-Vortex Problem

Imposed Period	2π
Domain of problem	$-\pi \leq x \leq \pi$
Length Scale L	Period/2π
Velocity Scale	$(gL)^{\frac{1}{2}}$
Time Scale	$(L/g)^{\frac{1}{2}}$
Location of Vortex	$(\frac{\pi}{10},\pi)$,$(-\frac{\pi}{10},\pi)$
Strength of Vortex	(100), (-100)

Table 3: Initial Conditions and Other Parameters for Free Surface-Vortex Problem

Domain of problem	$-67 \leq x \leq 67$
Damping Layer	$47 \leq \ \lvert x \rvert \ \leq 67$
Length sacle L	Initial Distance of Two Vortices
Velocity Scale	$(gL)^{\frac{1}{2}}$
Time Scale	$(L/g)^{\frac{1}{2}}$
Location of Vortex	(0.5,-5.0),(-0.5,-5.0)
Strength of Vortex	(2.236068),(-2.236068)

LIST OF FIGURES

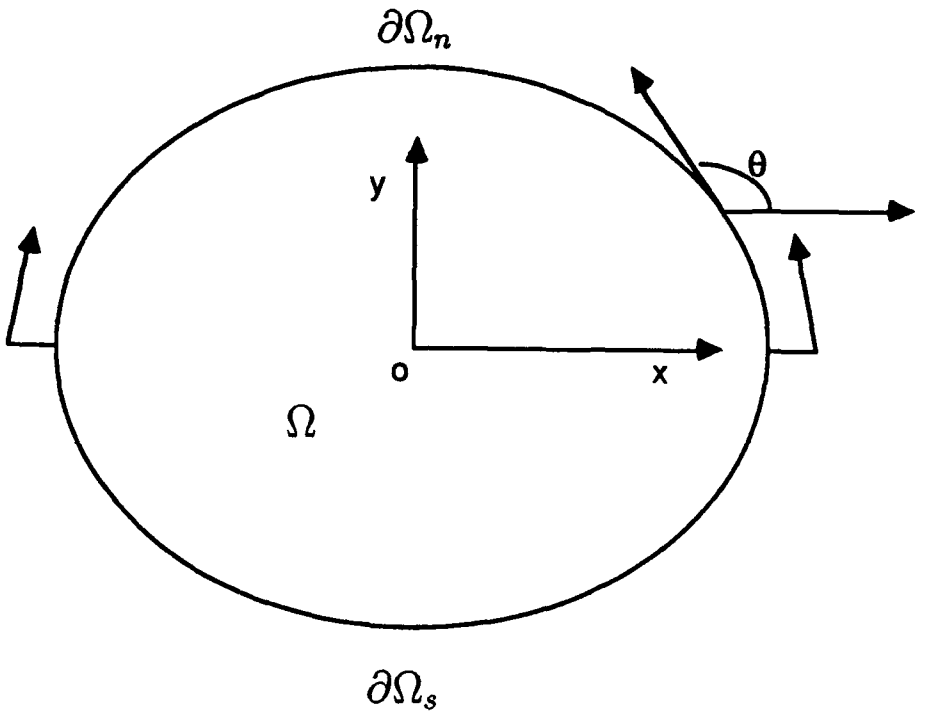

Figure 1: Domain and Bounding Surfaces

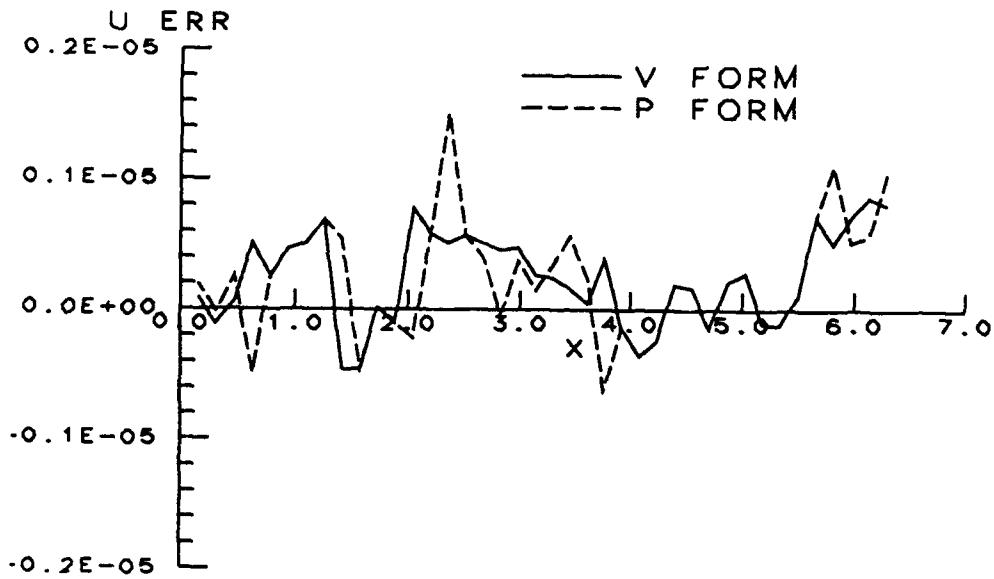

(a) x velocity

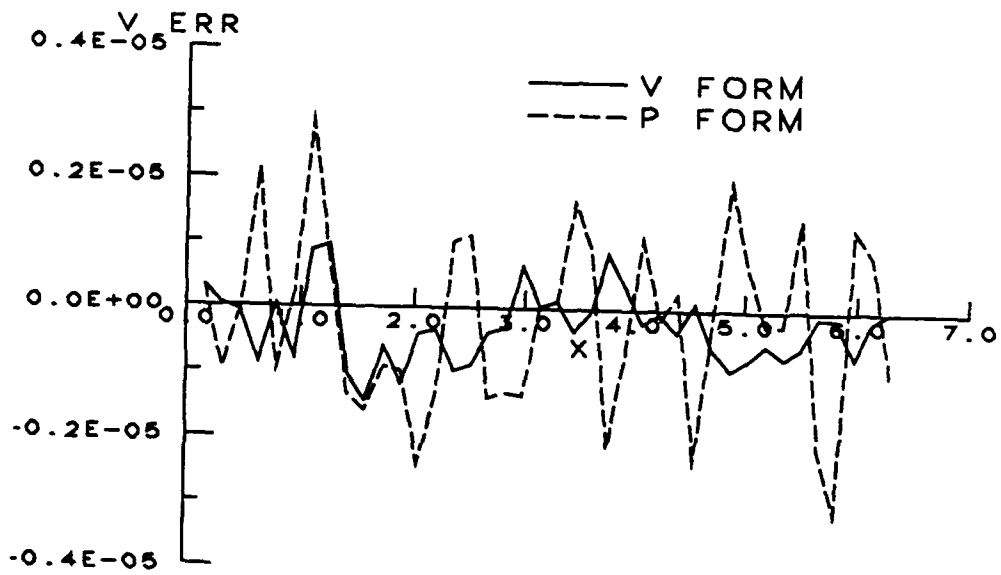

(b) y velocity

Figure 2: Comparison of Errors in Velocity between Two Methods (N=40,t=0.0)

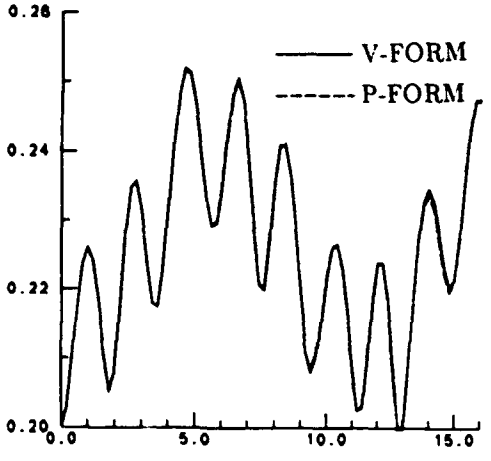

(a) Y_{max}

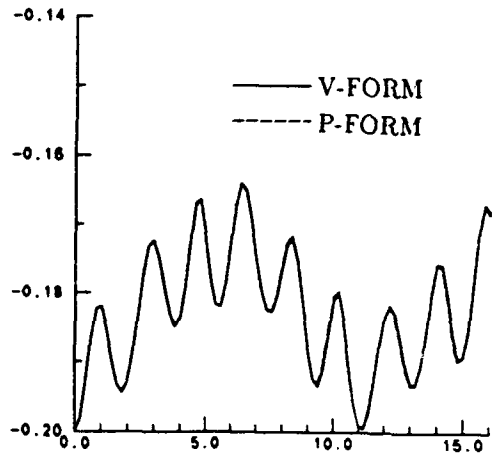

(b) Y_{min}

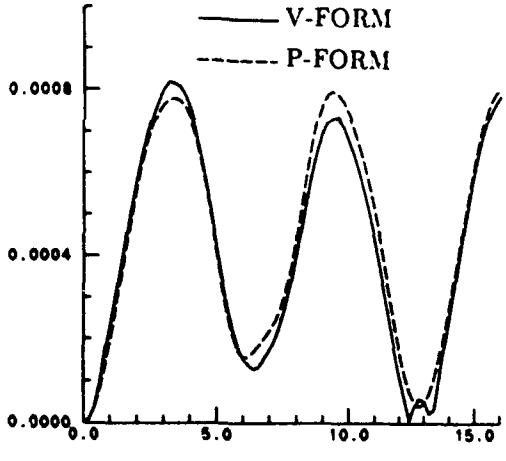

(c) E_m

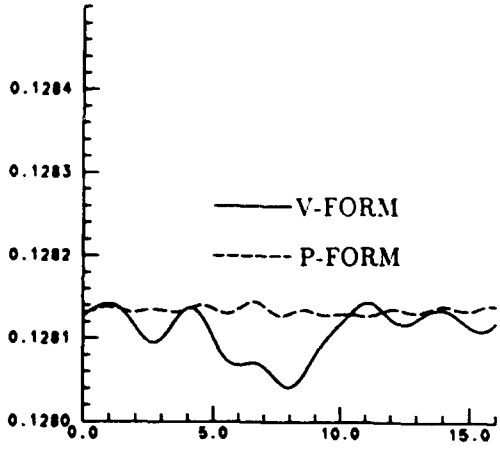

(d) $E(t)$

Figure 3: Variation of Y_{max}, Y_{min}, E_m, and $E(t)$ in Time (N=80, $\Delta t = 0.2$)

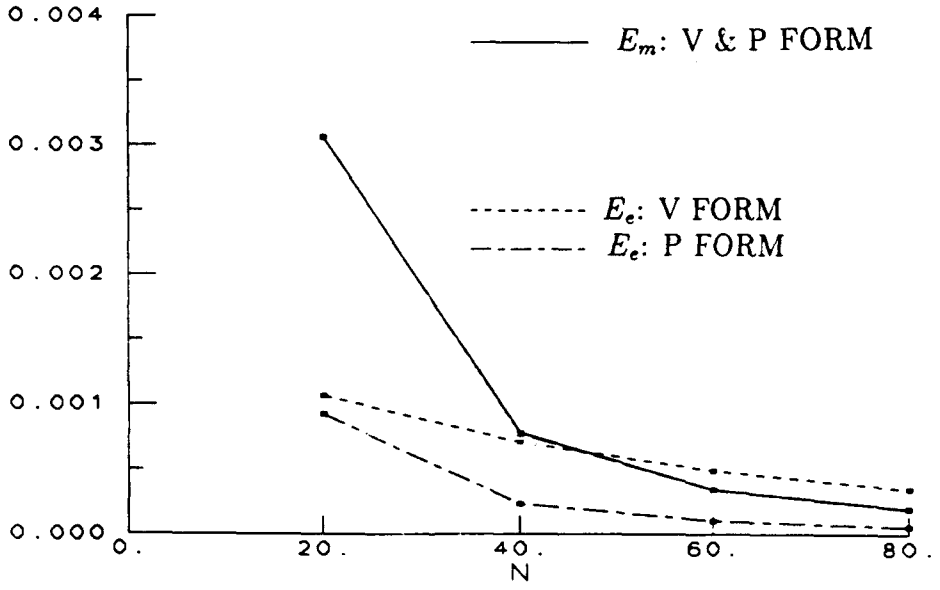

Figure 4: Results of Convergence Test for E_m, and E_e
($\Delta t = 0.1$, t=1.0)

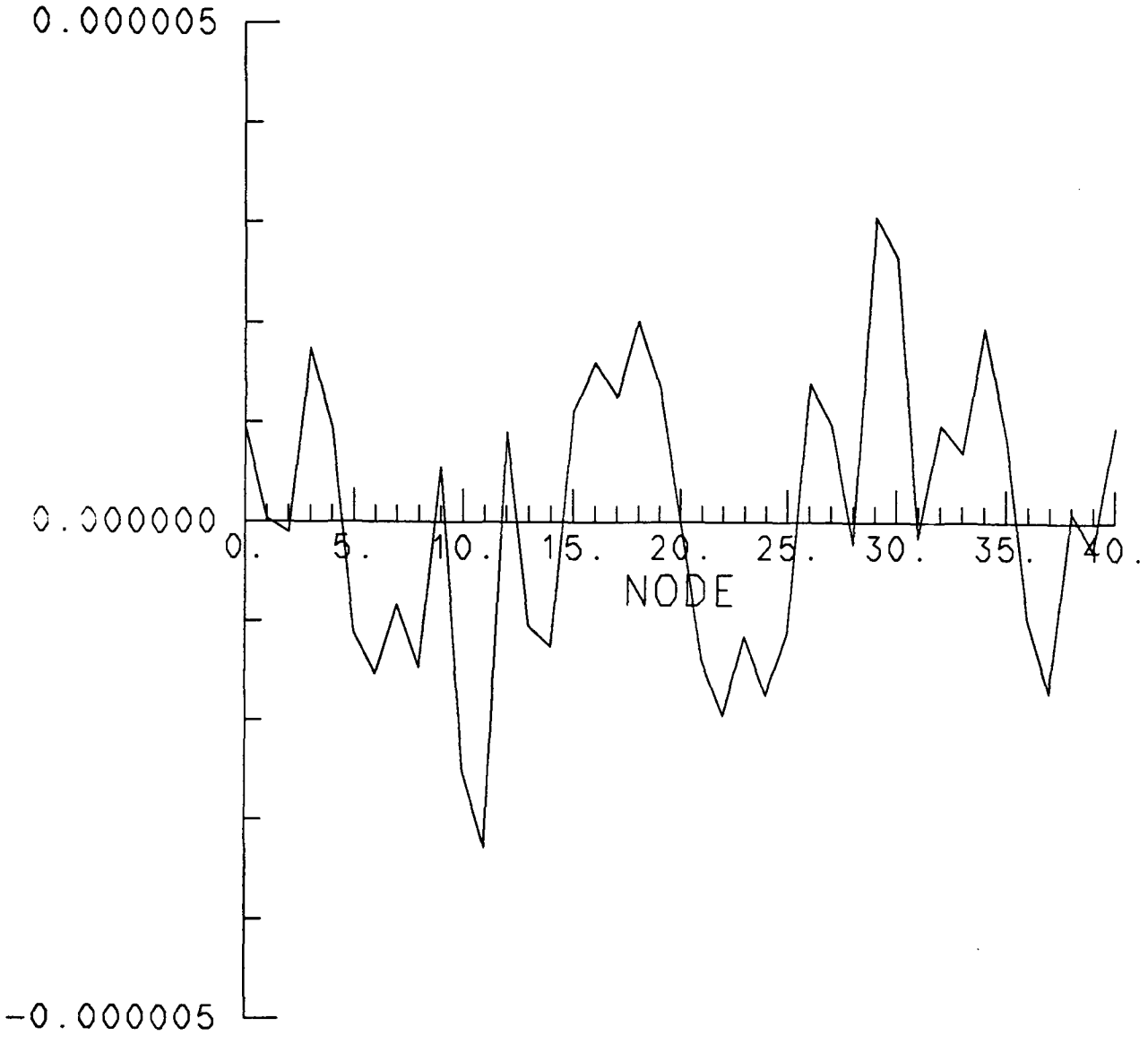

Figure 5: Error in Tangential Velocity for Wall-Vortex Problem (N=40,t=0.0)

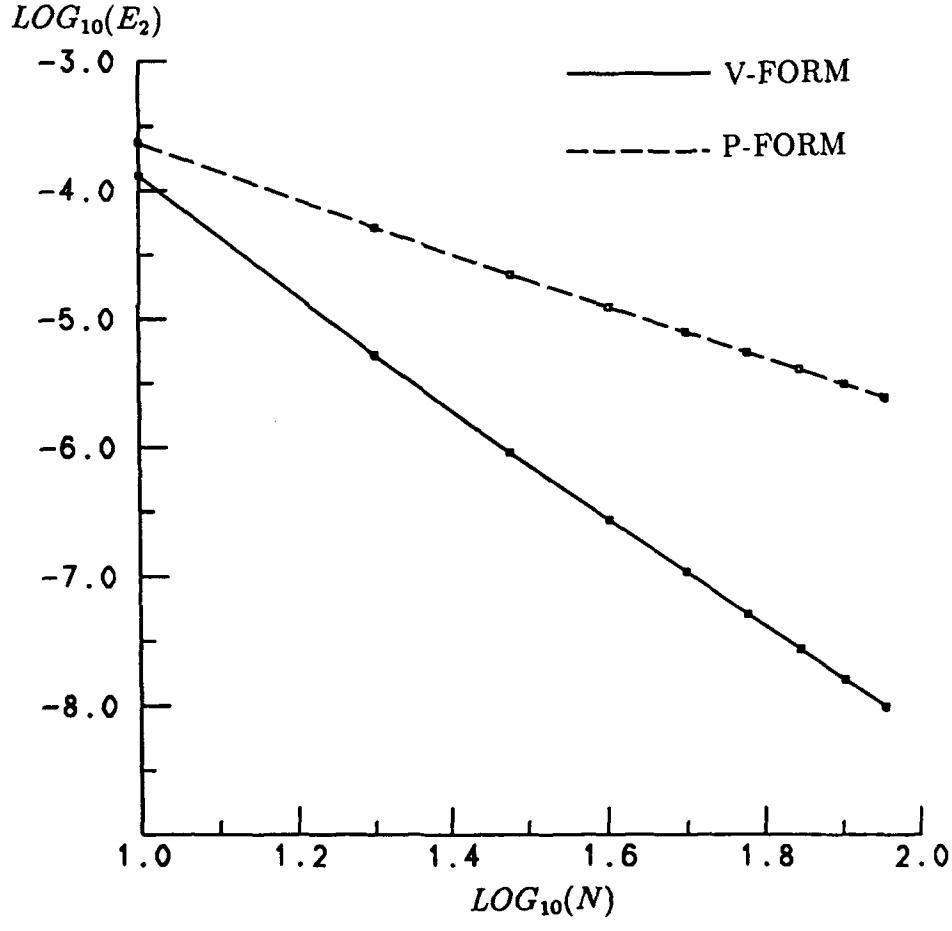

Figure 6: E_2 Errors in Tangential Velocity for Wall-Vortex Problem (t=0.0)

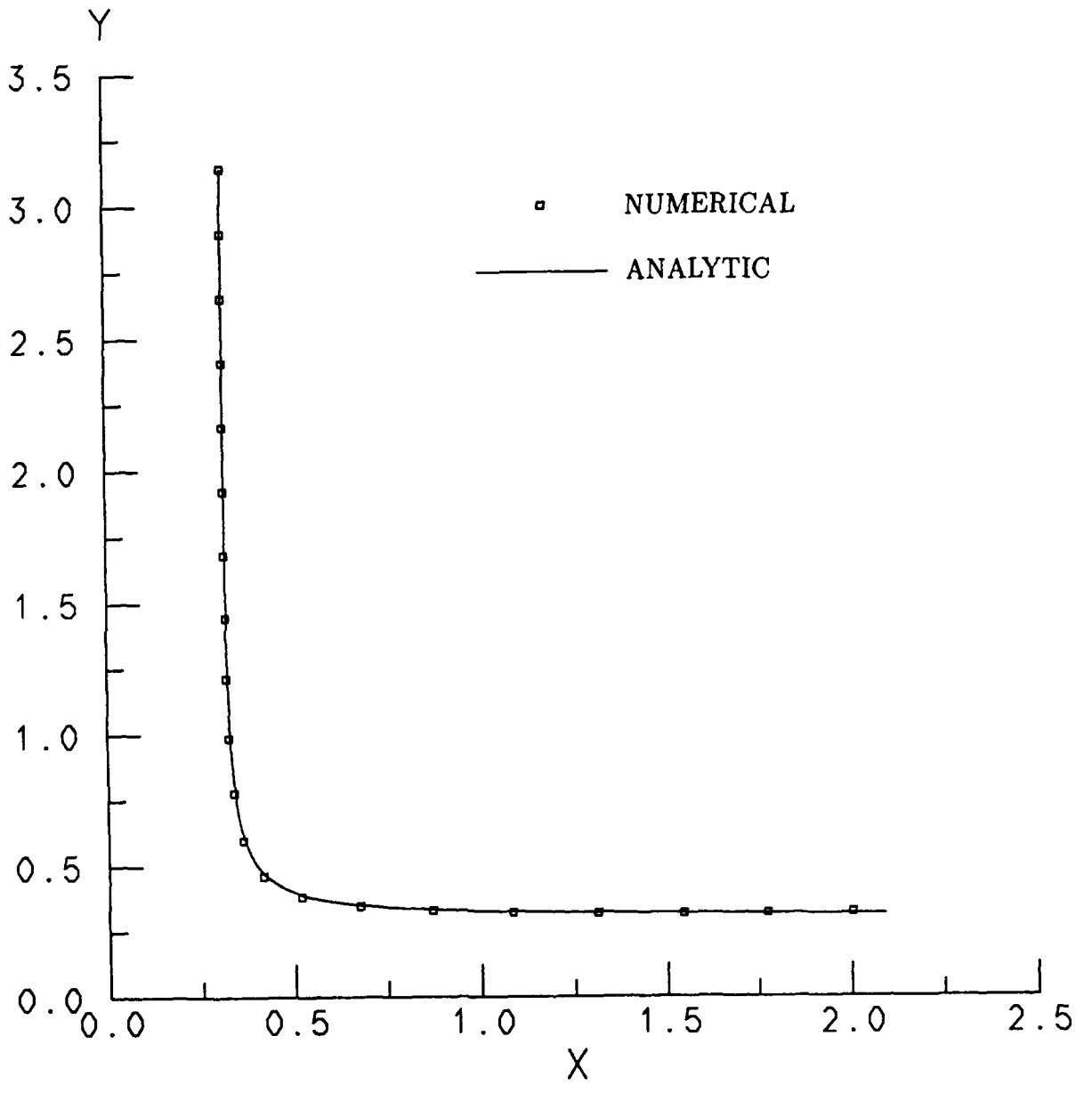

Figure 7: Locus of Vortex Motion

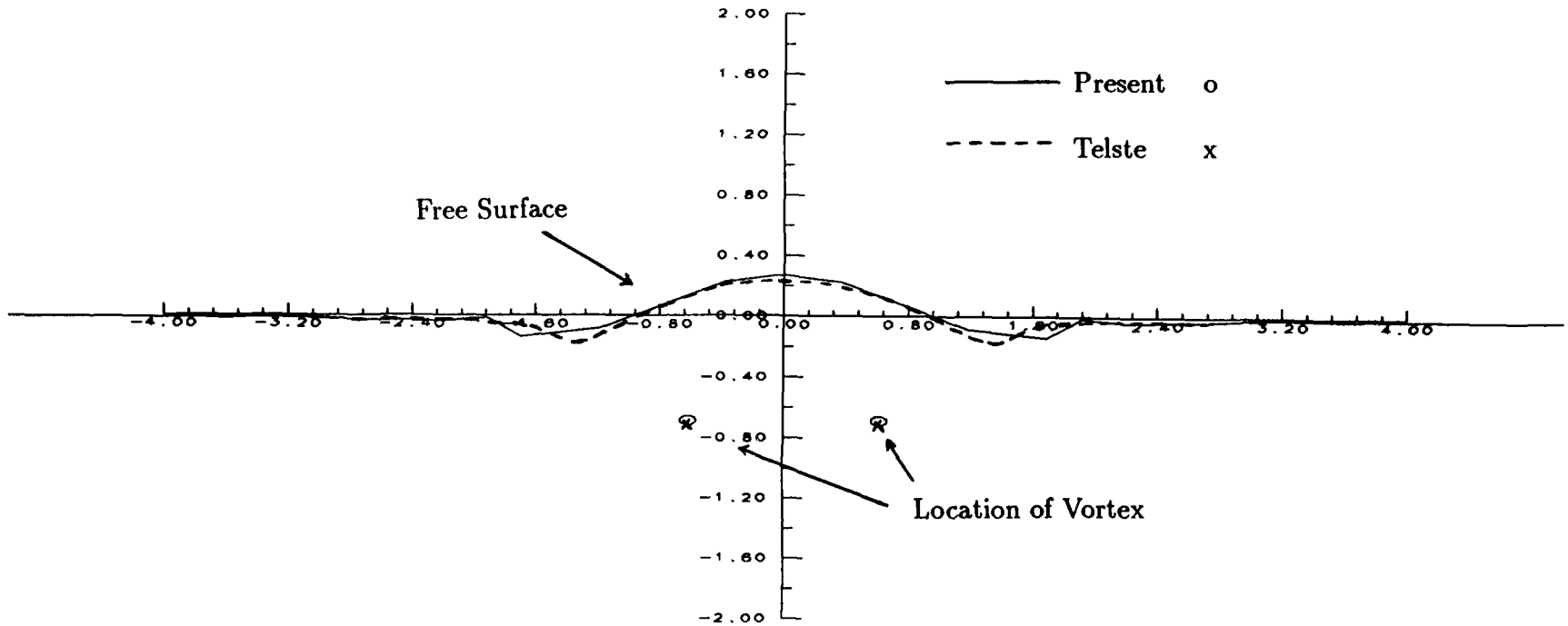

Figure 8: Free Surface Elevation at t=13.4164